

Impact of capillary rise orientation on sodium chloride-induced alteration of Rabat calcarenite stone

Mohammed Hraitia¹, Abdelaali Rahmouni^{2*}, Younes El Rhaffari³,
Yves Géraud⁴, Aziz Zaroual⁵

¹ Department of Physics, Higher Normal School, Mohammed V University, Rabat, Morocco

² Laboratory of Solid State Physics, Department of Physics, Faculty of Science Dhar El Mahraz, Sidi Mohamed Ben Abdellah University, Fez, Morocco

³ Laboratory of Civil Engineering and Environment, Higher School of Technology of Salé, Mohammed V University, Rabat, Morocco

⁴ University of Lorraine, ENSG, UMR 7359-GeoRessources, Nancy, France

⁵ Laboratory of Materials, Nanotechnologies and Environment, Faculty of Science, Mohammed V University, Rabat, Morocco

* Corresponding author's e-mail: abdelaali.rahmouni@usmba.ac.ma

ABSTRACT

The present work aims to investigate, through an experimental approach, the impacts of bedding plane orientation and salt concentration on the deterioration of calcarenite due to salt precipitation. This study concerns two sets of unaltered samples extracted parallel and perpendicular to the stratification plane. Imbibition-drying cycles were performed using sodium chloride saline solutions with concentrations of 15 g/L and 45 g/L. At the end of the test, various measurement and characterization techniques were used to analyze any changes in the samples. The results of capillary imbibition kinetics show that the stone's orientation with respect to the stratification plane, the salt concentration, and the material's porosity are critical factors influencing its weathering. Mercury porosimetry analysis further indicates that halite predominantly precipitates on the sample's surface, leading to efflorescence, while only a minimal or negligible amount of salt crystals forms within the porous media (subflorescence).

Keywords: historical monuments, calcarenite stone, porous media, porosity, mercury porosimetry, capillary imbibition kinetics.

INTRODUCTION

The crystallization of soluble salts within building materials represents a significant factor in their degradation, impacting both geological formations and built heritage (Balksten and Strandberg-de Bruijn, 2021; Cappai et al., 2024). Over time, stones deteriorate due to physico-chemical processes driven by salt activity, leading to various damage patterns. Stones with high porosity and rapid kinetics of imbibition and evaporation are particularly vulnerable to salt-induced damage (Ruedrich and Siegesmund, 2007; Shahidzadeh-Bonn, 2011). Limestone, in particular, is among the most susceptible rocks (Sánchez

et al., 2023; Abdi et al., 2024). The presence of salts, whether in soluble or hydrated forms, amplifies the potential for damage. The weathering process is influenced by environmental factors such as rain, wind, and atmospheric pollution, as well as the intrinsic properties of the stone itself. Over extended periods, these processes result in irreversible deterioration. Salt-related damage manifests in five primary forms: efflorescence, scaling, sanding, alveolization, and encrustations, as detailed in the ICOMOS glossary (2008).

Salts penetrate materials in solution and then crystallize following environmental changes (temperature, relative humidity). The deterioration, whose mechanisms have not yet been fully

elucidated, is related to the repetition of the dissolution-recrystallization cycle of salts within the material's porous network. This type of deterioration is often observed on traditional building materials (stone, brick, mortar, plaster, etc.), which constitute many historical monuments and archaeological sites where large quantities of salts may have accumulated over the centuries.

Over the years, several hypotheses and theoretical models have been proposed to explain how salts induce both aesthetic and, more critically, mechanical alterations in building materials. Among these, crystallization pressure has emerged as the most significant mechanism (Coussy, 2006; Desarnaud et al., 2016). This concept suggests that, during supersaturation, the growth of salt crystals generates a substantial pressure on the walls of the material's pores, referred to as crystallization pressure. Such pressure can reach magnitudes of several megapascals (La Iglesia et al., 1997; Derluyn and Prat, 2024) and may surpass the material's tensile strength, ultimately causing damage to its structural matrix (Espinosa-Marzal and Scherer, 2010).

The calcarenite stone has been used since antiquity in the construction of Moroccan historical monuments, spanning civilizations from the Phoenician, Carthaginian, and Roman periods to the later Almohad, Merinid, and Saadian eras. Its behavior and characteristics have been the subject of many research. Samaouali et al. (2010) investigated the processes of calcarenite degradation from the Chellah site, focusing on the porous media structure, fluid content, and the distribution, type, and quantity of clays present. Hraita et al. (2016) examined the effects of sediment bedding, salinity on salt precipitation, and porosity, as well as changes in calcarenite permeability and thermal properties during saturation and drying cycles. Vasanelli et al. (2021) analyzed the impact of a historical fire on calcarenite from a historic structure in Southern Italy, noting that the material's high porosity reduced microstructural damage, resulting in minimal changes to its physical properties. Rahmouni et al. (2023) studied the relationship between porosity, seismic, and thermal properties in dry and saturated calcarenite stones, identifying strong linear correlations while considering two primary anisotropy axes. In addition, Spairani-Berrio et al. (2023) evaluated the benefits of bioconsolidation treatments on calcarenite, observing significant enhancements in the

stone's petrophysical and mechanical properties after treatment.

This study aims to characterize calcarenite samples contaminated with sodium chloride using two complementary methods: capillary imbibition kinetics and mercury porosimetry. These techniques provide both qualitative and quantitative insights into structural modifications that may occur within the stone.

MATERIALS AND METHODS

Samples description

The material selected for this study is calcarenite stone, a coarse-grained bioclastic limestone commonly used in Morocco for construction and ornamental purposes. This sedimentary rock, known for its varied and heterogeneous texture, shows signs of deterioration such as alveolar weathering, scaling, sanding, as well as white and black crust formations. In addition, efflorescence and subflorescence are frequently observed on this stone in quarries, architectural structures, and monuments, particularly in coastal cities.

The physical and mechanical properties of calcarenite stone are influenced by its sedimentological characteristics, such as carbonate content and grain size, as well as petrographic features, including texture, cement percentage, and diagenetic processes (Asebry et al., 2007, Rahmouni et al., 2014). Calcarenites are characterized by high and variable porosity, ranging from 18% to 47% (Boulanouar et al., 2012; Rahmouni et al., 2013; El Rhaffari et al., 2014), coupled with relatively good compressive strength. However, the fracture strength test tested by the relative strength index shows that plio-quadernary calcarenites have low fracture strength with values ranging between 0.01 and 0.84 kN/cm² (Zaouia et al., 2014).

A calcarenite block from the Rabat quarry (Fig. 1a) was used to core 8 samples measuring 3.3cm in diameter and 5cm in height. Four of these samples were taken parallel to the bedding plane (series 1), while the remaining four were extracted perpendicular to it (series 2) (Fig. 1b). The block predominantly consists of calcium carbonate (CaCO₃) at 70.79%, with a minor silica (SiO₂) content of 6%, present as quartz grains (Hraita et al., 2014; Rahmouni et al. 2023). Samples from both series exhibit relatively high total porosity (22.44–29.61%), low trapped porosity

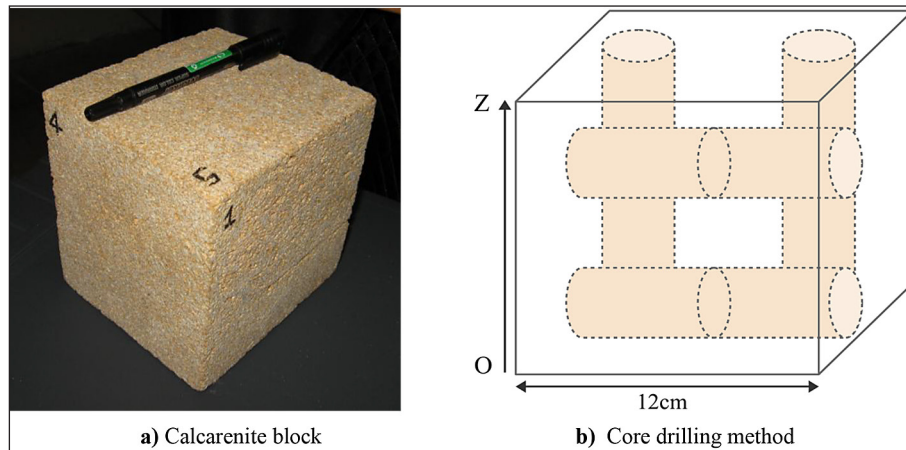


Figure 1. (a) A calcarenite block obtained from the Rabat quarry; (b) The core drilling process used to extract cylindrical specimens from the block. The OZ axis is oriented perpendicular to the bedding plane. Four specimens were extracted parallel to the bedding plane (Series 1), while another four were taken perpendicular to it (Series 2). Each specimen has a cylindrical shape with a diameter of 3.3 cm and a height of 5 cm

(2.14–4.12%), thermal conductivity values between 1.15 and 1.19 W/(m·K), and significant permeability ranging from 4.4 to 5.5 Darcy (Boulanouar et al. 2013).

Selection of contaminating salt

The selection of a contaminating salt is generally guided by environmental conditions and the specific objectives of the research. Commonly used salts in laboratory studies include sodium chloride, sodium sulfate, magnesium chloride, sodium nitrate, and others. It's important to note that each of these salts has unique effects on building due to differences in their chemical composition and interactions with the building materials. For instance, sodium chloride is frequently chosen because of its high solubility and common presence in marine and coastal environments, making it a relevant contaminant for studies on built heritage and historical monuments located in such areas. Nevertheless, the type of contaminating salt to use should always be based on a thorough analysis of the study site conditions and specific research objectives.

Sodium chloride has been widely identified as a significant contributor to salt-induced deterioration, particularly in monuments located in coastal

regions. In Rabat, several studies have focused on the citadel of Chellah, as well as the ramparts and gates of the old Medina (Zaouia et al., 2005; Samaouli et al., 2010). These investigations have highlighted the weathering of stone surfaces in these historic structures, attributing the primary cause of deterioration to the presence of sodium chloride (Table 1). The experimental technique for the salt crystallization test was based on protocol No. II.6 of the RILEM standard. The samples were placed vertically on a rack inside a tray, which was hermetically sealed with a cover to maintain near-saturation humidity levels. This setup minimized evaporation processes that could interfere with capillary action. The experiment was conducted in an air-conditioned room at a controlled temperature of 25 °C, with the saline solution in the tray maintained at a depth of approximately 3 mm. Two concentrations of sodium chloride (15 g/L and 45 g/L) were used. Following saturation, the samples were oven-dried at 60 °C for 48 hours until a constant dry weight was achieved. This process was repeated over five wetting-drying cycles.

Mercury porosimetry technique

Mercury intrusion porosimetry (MIP) was used to evaluate the total porosity of the samples.

Table 1. Concentrations of saline solutions used in the capillary rise method

Material	Cores parallel to the bedding plane (series 1)				Cores perpendicular to the bedding plane (series 2)			
	EP1	EP2	EP3	EP4	EH1	EH2	EH3	EH4
[NaCl] (g/L)	45	15	45	15	45	15	15	45

This method determines the pore size distribution by analyzing pressure-volume data. The measurements were carried out using a Micromeritics Pore Sizer 9320 porosimeter, which operates over a pressure range of 0.001 to 207 MPa, corresponding to pore sizes between 400 μm and 0.06 μm. The process involves two phases: a low-pressure measurement (0.001–0.150 MPa) and a high-pressure measurement (0.150–207 MPa). The relative uncertainty in the total porosity measurements is approximately 4% (Rahmouni et al., 2014).

RESULTS AND DISCUSSION

Upon completing the drying phase, halite crystals were observed forming on the surface of the samples, a phenomenon known as efflorescence. A small amount of salt also appeared to precipitate within the pore spaces. The resulting salt crust was notably thin and adhered tightly to the stone surface, making it challenging to remove. Over successive cycles, these efflorescences tended to accumulate, particularly in the lower regions of the samples due to the influence of gravity.

Imbibition kinetics

The kinetics of capillary imbibition has been studied in sedimentary rocks and granites. The capillary transfer properties of these rocks significantly impact the crystallization and dissolution of salts, which in turn affect the extent of material degradation (Zhao et al., 2020; Çetintaş et al., 2023). Figures 2 and 3 illustrate the progression of the solution mass absorbed by the samples throughout the imbibition-drying cycles.

The results indicate that the capillary imbibition rate during the imbibition-drying cycles is affected by the solution concentration, porosity

and the specimen sampling direction (parallel or perpendicular to the bedding plane). Specifically, for specimens extracted parallel to the bedding plane (series 1), the capillary imbibition rate remains nearly constant for $t < t_1$ across all applied cycles (Table 2), with $\Delta m/S$ showing no significant dependence on the cycles (Fig. 2). This suggests that the well-connected pore network, which is saturated first, does not experience any evolution relative to the number of cycles. However, for $t_1 < t$, there is a notable decrease in the capillary imbibition rate with increasing cycle number ($\Delta m/S$ decreases significantly from one cycle to another (Fig. 2). Consequently, the porous network saturated by the solution becomes less connected, leading to alterations in the pore structure presumably due to salt precipitation. The distribution of salt in the series 1 samples appears to be non-uniform. However, for samples taken perpendicular to the bedding plane (series 2), we observe that the capillary imbibition rate varies from the beginning of the experiment ($t \approx 0$) depending on the number of cycles (Table 2, Fig. 3). This suggests that the salt precipitates uniformly within the sample pore network (series 2), leading to a higher accumulation of salt in the samples of series 2 compared to those of series 1. These findings underscore the critical role of the stone’s orientation relative to the bedding plane in its susceptibility to alteration.

In what follows, our attention turns to mass saturation, denoting the mass of the solution impregnated in the sample at the end of the imbibition test (steady state). We have calculated the variation in the mass of solution captured in the saturation state during the applied cycles. The results are reported in Table 2. Thus, we observe that for all specimens taken parallel or perpendicular to the bedding plane (series 1 and 2), the ability to adsorb salt solution until saturation depends

Table 2. Solution weight gain values $\Delta m/S$ at time t_1 , where t_1 is the time at which the $\Delta m/S$ curves begin to deviate from one cycle to another (change in imbibition rate). $\Delta(\Delta m/S)$ is the variation during cycling of the mass in solution captured by the specimen after its saturation state

Parameters	Cores parallel to the bedding plane (series 1)				Cores perpendicular to the bedding plane (series 2)			
	EP1	EP2	EP3	EP4	EH1	EH2	EH3	EH4
[NaCl] en (g/L)	45	15	45	15	45	15	15	45
Water porosity (24 h)	15.98	16.38	18.27	18.86	19.35	16.31	19.29	17.16
Instant t_1 (min)	1	9	0.36	0.64	0	0	0.64	0.04
$\Delta m/S$ (g.cm ⁻²) at time t_1	0.25	0.4	0.35	0.4	0	0	0.3	0.06
$\Delta(\Delta m/S)$ (10 ⁻³ g.cm ⁻²) at saturation	20	10	48.7	46.8	14	10.1	30.3	49.6

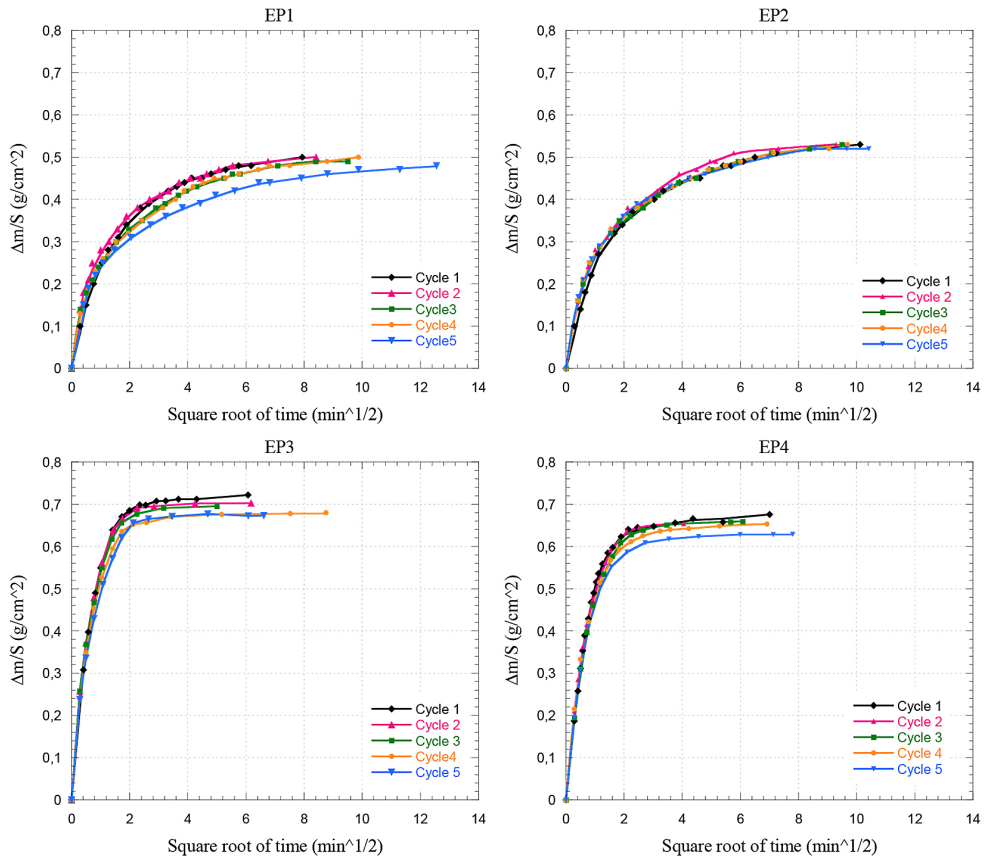


Figure 2. Solution weight gain curves for cores taken parallel to the bedding plane (series 1)

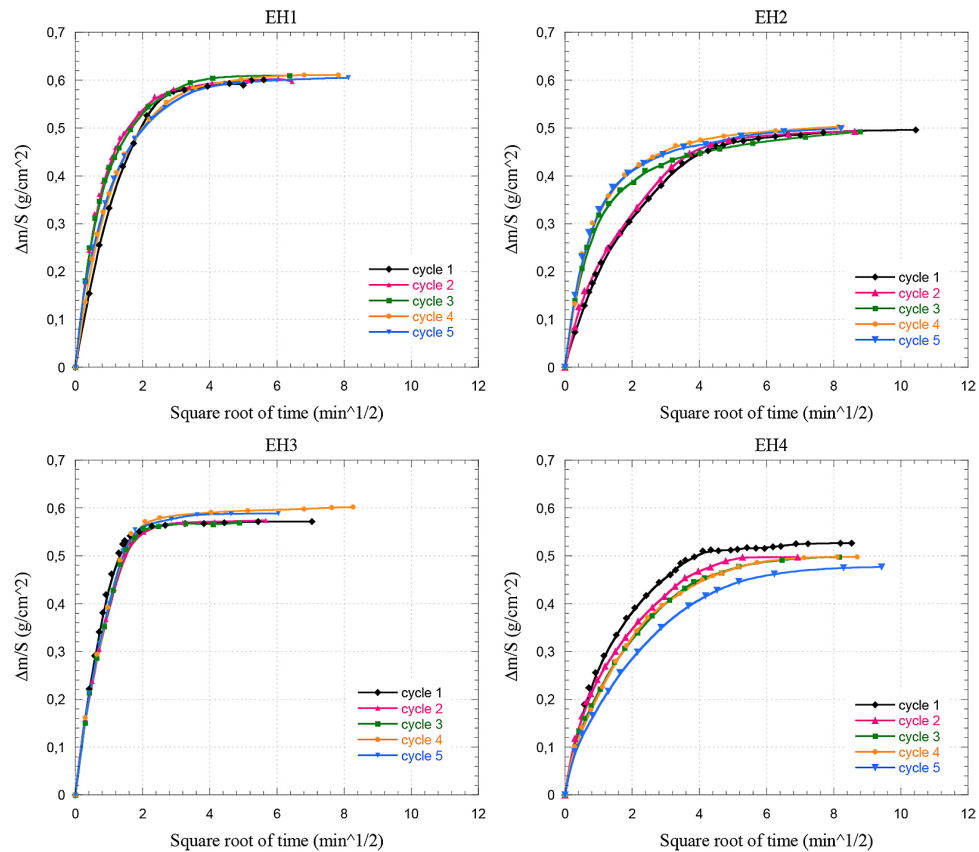


Figure 3. Solution weight gain curves for cores taken parallel to the bedding plane (series 2)

closely on both salt concentration and porosity. Indeed, the imbibition-drying tests conducted with the same NaCl concentration (45 g/L), on samples with varying porosities (EP1 and EP3), demonstrate that the variation $\Delta(\Delta m/S)$ increases considerably for higher porosity values. Additionally, other tests performed on specimens with identical porosity show that the variation $\Delta(\Delta m/S)$ increases significantly with the NaCl concentration (EH2 and EH4 for example). These results align well with those of the specific mass of precipitated salt (Hraita et al., 2016). This behavior could be explained by a decrease in porosity due to weathering and salt distribution in the stone's pore network. Overall, these results underscore the critical roles of salt concentration and porosity in the weathering process of stone materials.

Calcarenite stone in its healthy state appears to exhibit initial isotropy in its capillary transfer properties, depending on the orientation of its bedding plane (Hraita et al, 2014, Lubelli, et al., 2018). On the other hand, we have shown an anisotropic evolution of these properties during imbibition-drying cycles. This behavior can be attributed to variations in orientation and differences in the structure of the porous network specific to each sampling direction, whether parallel or perpendicular to the bedding plane. Indeed, calcarenite stone is a sedimentary stone characterized by the positioning of its quarry bed, which is linked to its sedimentation history, the rock having formed by stacking successive sediment layers. Given its high anisotropy, understanding the position of its sediment bed is crucial for any study. As a result, imbibition properties (pore size, connectivity, and tortuosity) stem directly from the capillary geometry of the porous network.

Consequently, the anisotropy of the material's structure and the connectivity of its porous network is characteristic of the anisotropy of capillary transfer properties and, consequently, of the stone's behavior during weathering cycles.

Mercury porosimetry

The pore distribution curves are shown in the Figures 4 and 5. The morphological study of pore access radius distribution spectra reveals no significant evolution below a threshold value of $1\mu\text{m}$. The finest pore spaces do not appear to be affected by the stresses imposed during the experimental cycles, regardless of the salt solution concentration or the orientation of the specimens relative to the bedding plane. On the contrary, significant changes appear in the range of pore sizes greater than $1\mu\text{m}$. This difference cannot be solely attributed to salt precipitation, as it is observed between the curves of the unaltered samples (EX1, EX2, EZ1 and EZ2). It is essentially due to the difference in the mesoporosity and macroporosity of the samples as a result of the overall heterogeneity of the material (Table 3).

These results show that sodium chloride crystals tend to precipitate on the sample surface (efflorescence), while a minor quantity of salt may possibly precipitate in the pore network. On the other hand, mercury porosimetry tests cannot clearly distinguish the preferred pore size for salt crystallization. Consequently, these analyses therefore provide little information on the specific role of microstructure in the alteration of calcarenite stone by sodium chloride.

Sodium chloride efflorescence can be partly explained by the fact that calcarenite stone is macroporous. Several studies have noted that stones with a higher proportion of micropores are more prone to salt-induced damage compared to those predominantly composed of macropores (Yang et al., 2020; Jia et al., 2024). On the other hand, Benavente et al (2004) have shown that for identical conditions of relative humidity and temperature, sodium chloride precipitates on the stone's surface (efflorescence), while sodium sulfate precipitates inside them (subflorescence).

Evaporation was carried out in the laboratory after capillary saturation, with samples placed

Table 3. Mercury porosimetry analysis results for unaltered samples in two orientations (EX and EZ)

Parameters	EX1	EX2	EZ1	EZ2
Total porosity (%)	29.61	24.48	27.90	22.44
Macroporosity (%)	23.05	19.73	22.62	17.09
Microporosity (%)	6.56	4.75	5.28	5.35
Threshold access diameter (μm)	156.79	156.86	156.69	156.67
Average pore diameter (μm)	3.078	2.404	1.985	1.530
Specific surface ($\text{m}^2\cdot\text{g}^{-1}$)	0.2047	0.2054	0.278	0.309

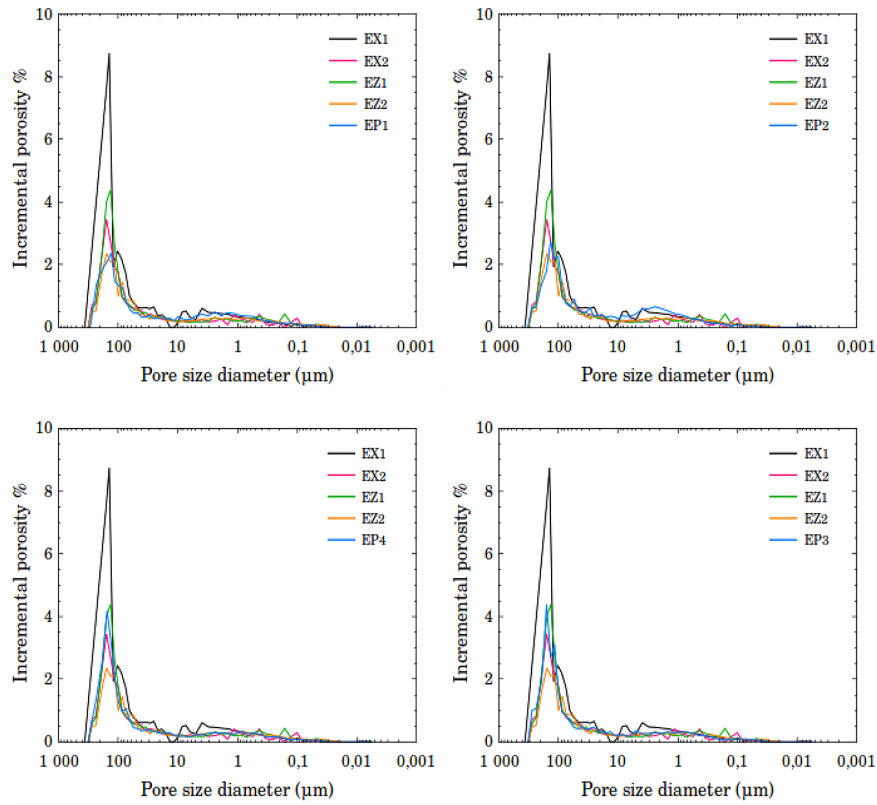


Figure 4. Mercury porosimetry curve for samples taken parallel to the bedding plane (series 1), compared with those of healthy samples (EX1, EX2, EZ1 and EZ2). The analysis is performed after five imbibition-drying cycles under the action of sodium chloride

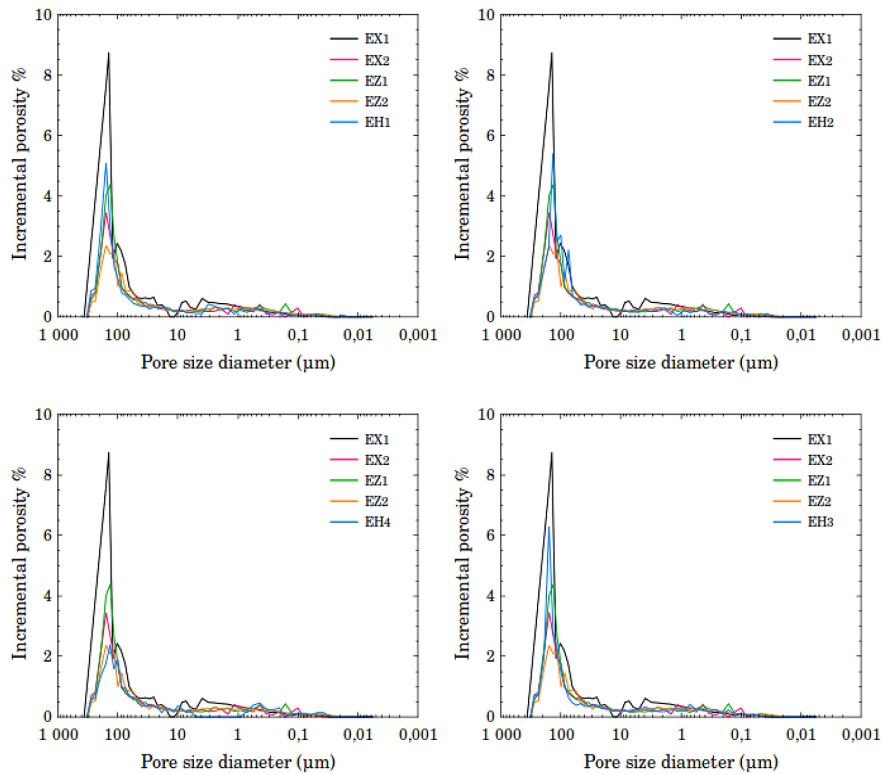


Figure 5. Mercury porosimetry curve for samples taken perpendicular to the sediment bedding (series 2), compared with those of healthy samples (EX1, EX2, EZ1 and EZ2). The analysis is performed after five imbibition-drying cycles under the action of sodium chloride

in the oven for each imbibition-drying cycle and subjected to a convective heating regime. Gomez-Heras and Fort (2007) have shown in a study conducted on sodium chloride-impregnated stones that the heating regime affects the localization of salt crystallization. Radiant heating effectively promotes subflorescence, while convective heating favors efflorescence. They also note that the use of a purely convective heating regime, in most laboratory experiments, results in an underestimation of the destructive potential of sodium chloride, a potential widely confirmed in real-world cases. This aligns with the fact that the crystallization pressure of sodium chloride does not create or enlarge cracks or pores in the tested samples.

Later, Samaouli et al. (2010) studied evaporation kinetics on three calcarenite specimens. These samples were cored from a calcarenite block from the Rabat quarry. The drying curves show that evaporation occurs actively on the surface and is less important at the depth of the stone. These characteristics are crucial in the degradation process by salt crystallization.

Other studies reveal that under the action of rapid evaporation, which does not allow the saline solution to migrate towards the stone's surface, deep penetration of the evaporation front into the stone is favored, resulting in subflorescence. However, if the evaporation rate is lower, the solution migrates more easily towards the external surface of the material, and the evaporation front remains localized on the surface, causing efflorescence.

CONCLUSIONS

In conclusion, this study highlights the complex processes involved in the weathering of calcarenite stone by salt precipitation. Through experimental investigations, we explored the influence of bedding plane orientation, salt concentration, and porosity on the alteration of calcarenite stone due to sodium chloride precipitation. Capillary imbibition kinetics revealed different material behaviors depending on the direction of capillary rise. Furthermore, mercury porosimetry analysis showed that for all the samples tested, the mercury intrusion curves exhibit the same pattern for access radii less than 59 μm . The samples then show comparable pore volumes. However, for access radii greater than 59 μm , the increment in injected mercury volume differs greatly from one sample to another. This difference arises because

the macroporosity varies from one sample to another due to the overall heterogeneity of the material. This suggests that halite crystals tend to precipitate on the sample surface (efflorescence), while a minority amount of salt may possibly precipitate within the porous network.

The observed efflorescence is partly due to the high macroporosity of the material and also to the use of a convective heating regime during drying. The latter leads to an underestimation of the destructive potential of sodium chloride, a potential that has been amply demonstrated in real cases.

Overall, this study underscores the importance of understanding the intrinsic properties of calcarenite stone, such as the orientation of its bedding plane and pore network structure, to predict and mitigate the effects of weathering. The results contribute to our understanding of salt-induced weathering mechanisms in calcarenite stone and offer valuable guidance for the preservation and conservation of stone structures in salt-rich environments. Further research in this area could explore additional factors influencing stone weathering and develop targeted mitigation strategies to safeguard cultural heritage assets.

REFERENCES

1. Abdi, Y., & Sabzi, M. (2024). The effect of salt crystallization on degradation of limestones used as heritage building stone in Lorestan, Iran. *Geoheritage*, 16, 118. <https://doi.org/10.1007/s12371-024-01019-8>
2. Asebriy, L., Cherkaoui, T. E., El Amrani El Hassani, I. E., Franchi, R., Guerrero, F., Martín-Martín, M., & Alcalá, F. J. (2009). Deterioration processes on archaeological sites of Chellah and Oudayas (World Cultural Heritage, Rabat, Morocco): Restoration test and recommendations. *Bollettino della Società Geologica Italiana*, 128(1), 157–171.
3. Balksten, K., & Strandberg-de Bruijn, P. (2021). Understanding deterioration due to salt and ice crystallization in Scandinavian massive brick masonry. *Heritage*, 4(1), 349–370. <https://doi.org/10.3390/heritage4010022>
4. Benavente, D., del Cura, M. G., García-Guinea, J., Sánchez-Moral, S., & Ordóñez, S. (2004). Role of pore structure in salt crystallisation in unsaturated porous stone. *Journal of Crystal Growth*, 260(3–4), 532–544. <https://doi.org/10.1016/j.jcrysgro.2003.09.004>
5. Boulanouar, A., Rahmouni, A., Boukalouch, M., Géraud, Y., El Hassani, I. E. A., Harnafi, M., &

- Sebbani, M. J. (2012). Correlation between P-wave velocity and thermal conductivity of heterogeneous and porous materials (in French). *MATEC Web of Conferences*, 2, 05004. <https://doi.org/10.1051/mateconf/20120205004>
6. Boulanouar, A., Rahmouni, A., Boukalouch, M., Samaouali, A., Géraud, Y., Harnafi, M., & Sebbani, J. (2013). Determination of thermal conductivity and porosity of building stone from ultrasonic velocity measurements. *Geomaterials*, 3(4), 138–144. <http://dx.doi.org/10.4236/gm.2013.34018>
 7. Cappai, M., Casti, M., & Pia, G. (2024). Salt crystallization in limestone: Materials decay and chemomechanical approach. *Materials*, 17(16), 3986. <https://doi.org/10.3390/ma17163986>
 8. Çetintaş, S., Bağcı, M., & Yıldız, A. (2023). Variations in capillary water absorption and porosity of some limestones during weathering due to salt and air pollutants. *Environmental Earth Sciences*, 82, 352. <https://doi.org/10.1007/s12665-023-11043-6>
 9. Coussy, O. (2006). Deformation and stress from in-pore drying-induced crystallization of salt. *Journal of the Mechanics and Physics of Solids*, 54(8), 1517–1547. <https://doi.org/10.1016/j.jmps.2006.03.002>
 10. Derluyn, H., & Prat, M. (Eds.). (2024). Salt crystallization in porous media. John Wiley & Sons.
 11. Desarnaud, J., Bonn, D., & Shahidzadeh, N. (2016). The pressure induced by salt crystallization in confinement. *Scientific Reports*, 6(1), 30856. <https://doi.org/10.48550/arXiv.1601.06585>
 12. El Rhaffari, Y., Hrait, M., Samaouali, A., Boukalouch, M., & Géraud, Y. (2014). Thermal and petrophysical characteristics of calcarenite rocks used in the construction of historical monuments of Rabat. *Romanian Journal of Materials*, 44(2), 153–159.
 13. Espinosa-Marzal, R. M., & Scherer, G. W. (2010). Mechanisms of damage by salt. *Geological Society, London, Special Publications*, 331(1), 61–77. <https://doi.org/10.1144/SP331.5>
 14. Gómez-Heras, M., & Fort, R. (2007). Patterns of halite (NaCl) crystallisation in building stone conditioned by laboratory heating regimes. *Environmental Geology*, 52, 259–267. <https://doi.org/10.1007/s00254-006-0538-0>
 15. Hrait, M., EL Rhaffari, Y., Fadili, G., Samaouali, A., Géraud, Y., & Boukalouch, M. (2016). Role of sediment bedding orientation and salt concentration on the evolution of petrophysical properties of calcarenite stone during salt weathering cycles by sodium chloride. *Romanian Journal of Materials*, 46(2), 242–249.
 16. Hrait, M., El Rhaffari, Y., Samaouali, A., Géraud, Y., & Boukalouch, M. (2014). Petrophysical, petrographical, and mineralogical characterization of calcarenite rock used for monumental building in Morocco. *Romanian Journal of Materials*, 44(4), 365–374.
 17. ICOMOS. (2008). Illustrated glossary on stone deterioration patterns.
 18. Jia, H., Yang, X., Wei, Y., Sun, Q., & Tang, L. (2024). Capillary imbibition laws of fresh–brackish waters in sandstone. *Water*, 16(8), 1180. <https://doi.org/10.3390/w16081180>
 19. La Iglesia, A., González, V., López-Acevedo, V., & Viedma, C. (1997). Salt crystallization in porous construction materials I: Estimation of crystallization pressure. *Journal of Crystal Growth*, 177(1–2), 111–118. [https://doi.org/10.1016/S0022-0248\(96\)01072-X](https://doi.org/10.1016/S0022-0248(96)01072-X)
 20. Lubelli, B., Cnudde, V., Diaz-Goncalves, T., Franzoni, E., van Hees, R. P., Ioannou, I., & Viles, H. (2018). Towards a more effective and reliable salt crystallization test for porous building materials: State of the art. *Materials and Structures*, 51, 1–21. <https://doi.org/10.1617/s11527-018-1180-5>
 21. Rahmouni, A., Boulanouar, A., Boukalouch, M., Géraud, Y., Samaouali, A., Harnafi, M., & Sebbani, J. (2013). Prediction of porosity and density of calcarenite rocks from P-wave velocity measurements. *International Journal of Geosciences*, 4, 1292–1299. <http://dx.doi.org/10.4236/ijg.2013.49124>
 22. Rahmouni, A., Boulanouar, A., Boukalouch, M., Samaouali, A., Géraud, Y., & Sebbani, J. (2014). Porosity, permeability, and bulk density of rocks and their relationships based on laboratory measurements. *Romanian Journal of Materials*, 44(2), 147–152.
 23. Rahmouni, A., Boulanouar, A., El Rhaffari, Y., Hrait, M., Zaroual, A., Géraud, Y., & Nabawy, B. S. (2023). Impacts of anisotropy coefficient and porosity on the thermal conductivity and P-wave velocity of calcarenites used as building materials of historical monuments in Morocco. *Journal of Rock Mechanics and Geotechnical Engineering*, 15(7), 1687–1699. <https://doi.org/10.1016/j.jrmge.2023.02.008>
 24. Rijniens, L. A., Huinink, H. P., Pel, L., & Kopinga, K. (2022). Experimental evidence of crystallization pressure in porous materials. *Journal of Applied Physics*, 131(4), 045101.
 25. Ruedrich, J., & Siegesmund, S. (2007). Salt and ice crystallisation in porous sandstones. *Environmental Geology*, 52(2), 225–249. <https://doi.org/10.1007/s00254-006-0585-6>
 26. Samaouali, A., Laânab, L., Boukalouch, M., & Géraud, Y. (2010). Porosity and mineralogy evolution during the decay process involved in the Chellah monument stones. *Environmental Earth Sciences*, 59, 1171–1181. <https://doi.org/10.1007/s12665-009-0106-5>
 27. Sánchez, M. A., Navacerrada, R., Fort, R., & Barbero-Barrera, M. M. (2023). Assessment of limestone cladding deterioration due to crystallisation of salts by non-destructive techniques. *Construction and Building Materials*, 400, 132640. <https://doi.org/10.1016/j.conbuildmat.2023.132640>

- org/10.1016/j.conbuildmat.2023.132640
28. Shahidzadeh-Bonn, N., Desarnaud, J., Bertrand, F., Chateau, X., & Bonn, D. (2010). Damage in porous media due to salt crystallization. *Physical Review E*, 81, 066110. <https://doi.org/10.1103/PhysRevE.81.066110>
29. Spairani-Berrio, Y., Huesca-Tortosa, J. A., Rodriguez-Navarro, C., Gonzalez-Muñoz, M. T., & Jroundi, F. (2023). Bioconsolidation of damaged construction calcarenites and evaluation of the improvement in their petrophysical and mechanical properties. *Materials*, 16(17), 6043. <https://doi.org/10.3390/ma16176043>
30. Vasanelli, E., Quarta, G., Micelli, F., & Calia, A. (2021). The effects of a historical fire on a porous calcarenite from an industrial-archaeological building in the south of Italy. *Engineering Geology*, 292, 106270. <https://doi.org/10.1016/j.enggeo.2021.106270>
31. Yang, L., Chen, C., Liu, Y., & Zheng, Y. (2020). A comparative study of ion diffusion during water imbibition in shale, sandstone, and volcanic rock. *Capillarity*, 3(2), 16–27. <http://dx.doi.org/10.46690/capi.2020.02.01>
32. Zaouia, N., El Wartiti, M., Nahraoui, F. Z., & Dabi, S. (2014). Study of the weathering of calcarenite in Rabat monuments: influence of atmospheric pollution and marine aerosols (in French). *MATEC Web of Conferences*, 11, 03015. <https://doi.org/10.1051/mateconf/20141103015>
33. Zaouia, N., Elwartiti, M., & Baghdad, B. (2005). Superficial alteration and soluble salts in the calcarenite weathering: Case study of Almohade monuments in Rabat, Morocco. *Environmental Geology*, 48, 742–747. <https://doi.org/10.1007/s00254-005-0013-3>
34. Zhao, F., Sun, Q., & Zhang, W. (2020). Combined effects of salts and wetting–drying cycles on granite weathering. *Bulletin of Engineering Geology and the Environment*, 79, 3707–3720. <https://doi.org/10.1007/s10064-020-01773-3>